

# A Computationally Efficient Method for Large-Scale Concurrent Mapping and Localization\*

John J. Leonard<sup>1</sup> and Hans Jacob S. Feder<sup>2</sup>

<sup>1</sup>Massachusetts Institute of Technology, Dept. of Ocean Engineering, Cambridge, MA 02139, U.S.A., jleonard@mit.edu

<sup>2</sup>Massachusetts Institute of Technology, Dept. of Ocean Engineering, Cambridge, MA 02139, U.S.A., hjfeder@alum.mit.edu

## Abstract

Decoupled stochastic mapping (DSM) is a computationally efficient approach to large-scale concurrent mapping and localization. DSM reduces the computational burden of conventional stochastic mapping by dividing the environment into multiple overlapping submap regions, each with its own stochastic map. Two new approximation techniques are utilized for transferring vehicle state information from one submap to another, yielding a constant-time algorithm whose memory requirements scale linearly with the size of the operating area. The performance of two different variations of the algorithm is demonstrated through simulations of environments with 110 and 1200 features. Experimental results are presented for an environment with 93 features using sonar data obtained in a 3 by 9 by 1 meter testing tank.

## 1. Introduction

The objective of concurrent mapping and localization (CML) is to enable a mobile robot to build a map of an unknown environment while concurrently using that map to navigate. CML has been a central research topic in the field of mobile robotics due to its theoretical challenges and critical importance for applications [1, 2, 3]. Our approach is based on stochastic mapping (SM), a feature-based approach to CML first developed by Smith *et al.* [4] and Moutarlier and Chatila [5]. One of the key issues that has hampered previous work in feature-based CML is the map scaling problem [6]. The computational complexity of stochastic mapping is  $\mathcal{O}(n^2)$ , where  $n$  is the number of features in the environment [5]. This complexity arises from the need to represent an ever-growing number of correlations between the vehicle and the features in the map as the size of the map increases. Previous research has demonstrated that simple strategies which ignore correlations will become overconfident and di-

verge [7, 8].

In decoupled stochastic mapping (DSM), the environment is represented in terms of multiple globally-referenced submaps, each with its own vehicle track. Two new approximation methods, referred to as (1) cross-map vehicle relocation and (2) cross-map vehicle updating, are developed for transferring vehicle state estimate information from one submap to another as the vehicle transitions between map regions. These transition strategies are utilized to realize two variations of the DSM algorithm, single-pass DSM and multi-pass DSM. Using single-pass DSM, the error bounds do not improve with time and they become larger for submap regions that are further from the origin. In contrast, the multi-pass DSM method can achieve spatial convergence across all submaps.

## 2. Stochastic Mapping

We consider the scenario of an autonomous underwater vehicle (AUV) using forward-looking sonar to perform CML in an environment consisting of point-like features [9, 10]. In our implementation, the AUV senses features in the environment through range and bearing measurements. These measurements are used to create a map of the environment and concurrently to localize the vehicle. The complete full covariance algorithm, incorporating data association and track initiation, is referred to as augmented stochastic mapping (ASM) and is illustrated in Figure 1. More detail is provided in Feder *et al.* [10, 11].

The estimated locations of the robot and the features in the map are represented by a single state vector  $\hat{\mathbf{x}}[k] = [\hat{\mathbf{x}}_r[k]^T \ \hat{\mathbf{x}}_f[k]^T]^T$  at each discrete time step  $k$ , where  $\hat{\mathbf{x}}_r[k]^T$  and  $\hat{\mathbf{x}}_f[k]^T = [\hat{\mathbf{x}}_1[k]^T \ \dots \ \hat{\mathbf{x}}_N[k]^T]^T$  are the estimated robot and feature locations, respectively. Associated with this state vector is an estimated error covariance,  $\mathbf{P}[k]$ , which represents the errors in the robot and feature locations, and the cross-correlations

---

\*To appear in "Robotics Research: the Ninth International Symposium", John Hollerbach and Dan Koditschek (Eds), Springer-Verlag, London, 2000.

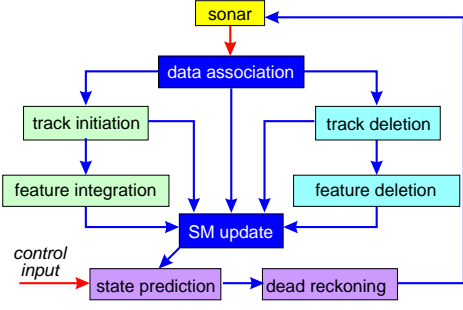


Figure 1: Augmented stochastic mapping (ASM) [11].

between these states:

$$\mathbf{P}[k] = \begin{bmatrix} \mathbf{P}_{rr}[k] & \mathbf{P}_{rf}[k] \\ \mathbf{P}_{fr}[k] & \mathbf{P}_{ff}[k] \end{bmatrix}. \quad (1)$$

We denote the vehicle's state by  $\mathbf{x}_r = [x_r \ y_r \ \phi \ v]^T$  to represent the vehicle's east position, north position, heading, and speed, respectively. The state of feature  $i$  is represented by  $\mathbf{x}_i = [x_i \ y_i]^T$ . The dynamic model used in the algorithm simulates an AUV equipped with control surfaces and a single aft thruster for propulsion, moving at a nominal forward speed of 2.5 m/s. The control input  $\mathbf{u}$  to the vehicle is given by a change in heading,  $\delta\phi$ , and speed,  $\delta v$ , of the vehicle to model changes in rudder angle and forward thrust, that is,  $\mathbf{u}[k] = [\delta\phi \ \delta v]^T$ . Thus, the dynamic model of the AUV,  $\mathbf{f}()$ , is given by

$$\mathbf{x}[k+1] = \mathbf{f}(\mathbf{x}[k], \mathbf{u}[k]) + \mathbf{d}_x(\mathbf{u}[k]), \quad (2)$$

where  $\mathbf{d}_x(\mathbf{u}[k])$  is a white, Gaussian random process independent of  $\mathbf{x}[0]$ .

The observation model  $\mathbf{h}()$  for the system is given by

$$\mathbf{z}[k] = \mathbf{h}(\mathbf{x}[k]) + \mathbf{d}_z, \quad (3)$$

where  $\mathbf{z}[k]$  is the observation vector of range and bearing measurements. The observation model,  $\mathbf{h}()$ , defines the (nonlinear) coordinate transformation from state to observation coordinates. The stochastic process  $\mathbf{d}_z$ , is assumed to be white, Gaussian, and independent of  $\mathbf{x}[0]$  and  $\mathbf{d}_x$ , and has covariance  $\mathbf{R}$ . Given these assumptions, an extended Kalman filter (EKF) is employed to estimate the state  $\hat{\mathbf{x}}$  and covariance  $\mathbf{P}$ .

### 3. Decoupled Stochastic Mapping

To overcome the  $\mathcal{O}(n^2)$  complexity of the EKF, the DSM algorithm divides the environment into multiple globally-referenced submap regions. Each submap has its own vehicle position estimate, a set of feature es-

timates and a corresponding estimated covariance matrix. The state estimate of the vehicle and all the features of submap  $A$  at time  $k$  is represented by  $\hat{\mathbf{x}}^A[k]$ . The covariance is represented by  $\mathbf{P}^A[k]$ :

$$\mathbf{P}^A[k] = \begin{bmatrix} \mathbf{P}_{rr}^A[k] & \mathbf{P}_{rf}^A[k] \\ \mathbf{P}_{fr}^A[k] & \mathbf{P}_{ff}^A[k] \end{bmatrix}. \quad (4)$$

In the current implementation, the size and location of each submap region is specified *a priori* based on an assumed density of features. Submap regions overlap slightly to prevent excessive map switching. If the vehicle travels into an area for which no submap exists, a new submap is created. If the vehicle travels into a previously visited region, then the earliest created submap containing the current estimated vehicle location is retrieved and either cross-map relocation or cross-map updating is performed.

To illustrate this process, suppose that the vehicle leaves submap  $A$  at time  $k$  and reenters submap  $B$ . Let  $j$  designate the most recent time step at which  $B$  was the active submap. Cross-map relocation performs the following steps:

$$\hat{\mathbf{x}}^B[k] \leftarrow \begin{bmatrix} \hat{\mathbf{x}}_r^A[k] \\ \hat{\mathbf{x}}_f^B[j] \end{bmatrix}, \quad \mathbf{P}^B[k] \leftarrow \begin{bmatrix} \mathbf{P}_{rr}^A[k] + \mathbf{P}_{rr}^B[j] & \mathbf{P}_{rf}^B[j] \\ \mathbf{P}_{fr}^B[j] & \mathbf{P}_{ff}^B[j] \end{bmatrix}.$$

The vehicle state estimate in submap  $B$  at time  $k$  is obtained by using the current vehicle state estimate from submap  $A$  and the feature state estimate from submap  $B$  from time step  $j$ . The current vehicle covariance from submap  $A$  is added to the vehicle covariance for submap  $B$  from time  $j$ , and the vehicle-to-feature correlation and feature covariance terms for submap  $B$  are left unchanged.

The goal of cross-map updating is to bring more accurate vehicle estimates from lower to higher maps, to facilitate spatial convergence. It consists of two steps, (1) de-correlation (denoted by  $k^-$ ) and (2) EKF updating (denoted by  $k^+$ ). First, the vehicle state estimate for submap  $B$  is randomized, the vehicle covariance for submap  $B$  is greatly inflated, and the feature covariance for submap  $B$  is doubled:

$$\hat{\mathbf{x}}^B[k^-] \leftarrow \begin{bmatrix} \phi^B \\ \mathbf{x}_f^B[k] \end{bmatrix}, \quad \mathbf{P}^B[k^-] \leftarrow \begin{bmatrix} \mathbf{P}_{rr}^B[j] + \Phi^B & \mathbf{P}_{rf}^B[j] \\ \mathbf{P}_{fr}^B[j] & 2\mathbf{P}_{ff}^B[j] \end{bmatrix},$$

where  $\phi^B$  designates a random value uniformly distributed over the region defining submap  $B$  and  $\Phi^B$  designates a covariance much larger than the size of submap  $B$ . Second, the vehicle state estimate from submap  $A$ ,  $\hat{\mathbf{x}}_r^A[k]$ , is used as a measurement  $\mathbf{z}$ , with

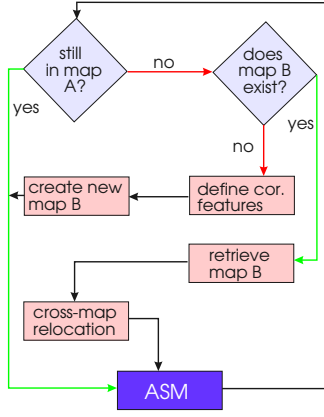


Figure 2: Single-pass decoupled stochastic mapping algorithm. Cross-map vehicle relocation is used for all transitions between submaps.

covariance  $\mathbf{P}_{rr}^A[k]$ , in an extended Kalman filter to update the vehicle position in submap  $B$ . This can be summarized by the following equations:

$$\begin{aligned} \mathbf{K} &= \mathbf{P}^B[k^-] \mathbf{H}^T (\mathbf{H} \mathbf{P}^B[k^-] \mathbf{H}^T + \mathbf{P}_{rr}^A[k])^{-1} \\ \hat{\mathbf{x}}^B[k^+] &\leftarrow \hat{\mathbf{x}}^B[k^-] + \mathbf{K}(\mathbf{z} - \mathbf{H} \hat{\mathbf{x}}^B[k^-]) \\ \mathbf{P}^B[k^+] &\leftarrow (\mathbf{I} - \mathbf{K} \mathbf{H}) \mathbf{P}^B[k^-] (\mathbf{I} - \mathbf{K} \mathbf{H})^T + \mathbf{K} \mathbf{P}_{rr}^A[k] \mathbf{K}^T \end{aligned}$$

where  $\mathbf{H}$  is the 4 by  $(4 + 2N)$  matrix  $[\mathbf{I} \ 0]$ . More detail is provided in [12].

Single-pass DSM uses cross-map relocation for all submap transitions, and is summarized in Figure 2. A constant time algorithm is obtained, because no operations need to be performed on the state estimates for inactive submaps. However, once a submap is created, the initial error present in the map can never be reduced, and spatial convergence does not occur. To slow the growth of spatial errors, a small number of features (called correspondence features) are included from the previous submap when a new submap is initialized [12].

Multi-pass DSM is summarized in Figure 3, and uses cross-map updating to transition from lower to higher submaps, and cross-map relocation to transition from higher to lower submaps. As the vehicle makes repeated passes through the environment, the error bounds of all submaps converge.

#### 4. Comparison Between DSM and Full Covariance Stochastic Mapping

To compare each DSM method with the ASM full covariance algorithm, simulations were performed for a scenario with 110 features randomly distributed over a 1 km by 1 km area, in the presence of clutter and

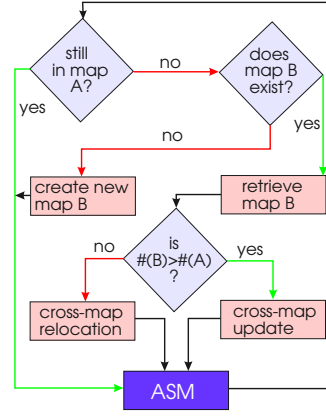


Figure 3: Multi-pass decoupled stochastic mapping. Cross-map vehicle relocation is used when transitioning from higher to lower maps, and cross-map vehicle updating is used when transitioning from lower to higher maps.

Table 1: Simulation parameters.

sampling period, $T$	1 sec.
maximum sonar range	200 m
sonar coverage angle	$\pm 40^\circ$
range measurement standard deviation	0.5 m
bearing measurement standard deviation	$5^\circ$
feature probability of detection	0.90
vehicle cruise speed	2.5 m/s
speed process standard deviation	5% of $\delta u$
heading process standard deviation	$2.0^\circ$
dead reckoning speed standard deviation	0.4 m/s
dead reckoning heading standard deviation	$3.0^\circ$
initial position uncertainty std. dev.	0.7 m
initial heading uncertainty std. dev.	$5.0^\circ$
initial speed uncertainty std. dev.	0.2 m/s
gate parameter $\gamma$	9
clutter parameter $\lambda$	1
track initiation parameters	$M = 5, N = 4$

dropouts. The desired path of the AUV and the true feature locations are shown in Figure 4.

The top two plots of Figure 5 show the position errors of the vehicle versus time and the  $3\sigma$  error bounds for ASM. On the first pass through the environment, the uncertainty grows as the vehicle is furthest from the origin, and then decreases when the vehicle returns close to the origin. On subsequent traversals, the error bounds are reduced.

For each of the two DSM algorithms, the survey area is partitioned into four submaps. Each submap bounds a 525 m by 525 m square region. Figure 4 shows the location of the submaps as generated by the DSM algorithm. The numbers signify the order in which submaps were created.

The middle plots of Figure 5 show the position errors for single-pass DSM. As with the full covari-

ance algorithm, the position uncertainty of the vehicle grows as the distance from the starting point increases. Further, after the first pass through the survey path, the ASM and the single-pass DSM results look very similar and achieve close to the same error bounds. The crucial difference between the methods is that ASM estimates the correlations between all features, while single-pass DSM only estimates the correlations within submaps. ASM is able to exploit all the correlations and thus reduce the global error at all locations. Single-pass DSM is unable to reduce the global uncertainty of submaps below the uncertainty upon creation of the submap. This can be seen from the “steps” in the north and east  $3\sigma$  bounds after the completion of the first pass through the survey area (that is, after the first 2 hours of the mission).

The bottom plots of Figure 5 show the position errors of the vehicle versus time and the  $3\sigma$  bounds for the survey performed by multi-pass DSM. The multi-pass errors resemble the results for ASM more than the results from single-pass DSM. Clearly, the vehicle does better after the first pass through the survey area (that is, after about 2 hours) than before. Thus, the algorithm is capable of reducing the *global* error everywhere and not only locally in the submaps, as for single-pass DSM. However, one can see that the error bounds are a little more uneven than those of ASM, and reducing the uncertainties takes a little more time.

## 5. Large-Scale Simulation Results

Next, we will demonstrate results using single-pass DSM and multi-pass DSM for surveying a large-scale environment with 1200 features for a mission duration of over 100 hours, sampling at a rate of 1 Hz. Figure 6 shows the desired path of the AUV through the 3 km by 3 km survey area, the partition of the survey area into submaps, and true and estimated positions of the features in the survey area for the multi-pass DSM simulation shown in Figure 8.

Figure 7 shows plots of the position errors of the vehicle versus time and the  $3\sigma$  bounds when using single-pass DSM for the survey area of Figure 6. In this simulation, the vehicle completed 11 laps of the survey path. The position uncertainty of each submap grows as a function of submap number.

Figures 8 and 9 show the position errors of the vehicle versus time when using multi-pass DSM for two different survey paths. In Figure 8, the vehicle follows the survey path indicated in Figure 6, whereas in Figure 9 the vehicle follows an alternating survey path that rotates the path given in Figure 6 by 90 degrees after

Table 2: DSM experiment parameters.

sampling period, $T$	1 sec.
maximum sonar range	250 cm
sonar coverage angle	$\pm 40^\circ$
range measurement standard deviation	2 cm
bearing measurement standard deviation	$5^\circ$
feature probability of detection	0.90
vehicle cruise speed	10 cm/s
speed process standard deviation	5% of $\delta v$
heading process standard deviation	$2.0^\circ$
dead reckoning speed standard deviation	0.45 cm/s
dead reckoning heading standard deviation	$3.0^\circ$
initial position uncertainty std. dev.	0.7 cm
initial heading uncertainty std. dev.	$5.0^\circ$
initial speed uncertainty std. dev.	0.2 cm/s
gate parameter $\gamma$	9
clutter parameter $\lambda$	1
track initiation parameters	$M = 5, N = 4$

each complete circuit of the environment.

The multi-pass DSM shows a considerable improvement over single-pass DSM in the long run as the survey area is revisited. However, during the first pass through the survey area, the maximum uncertainty when using multi-pass DSM is more than 30% higher than the result when using single-pass DSM. Single-pass DSM should be used when the survey area is to be traversed only once and multi-pass DSM should be used if one anticipates multiple traversals of the environment.

The normalized squared state errors [13] for the vehicle state estimates are also shown in Figures 7, 8, and 9. The normalized squared errors are reasonably well-behaved for the single-pass DSM run. However, Figure 8 indicates when the same repetitive survey path is used with multi-pass DSM, the amount of normalized squared errors falling outside the 99% error bounds is unacceptably high. However, this situation improves tremendously when the vehicle follows an alternating survey path, as illustrated by the mission shown in Figure 9. When the vehicle is able to observe each feature from many different survey directions, the normalized errors are very well-behaved.

## 6. Testing Tank Experiment

We now present a simple multi-pass DSM experiment for further investigation of the approach. The parameters for the mission were chosen so as to simulate an AUV scaled down by a factor of 100. A 500 kHz mechanically scanned sonar was mounted on a robotic positioning system and scanned over a  $\pm 40^\circ$  sector at each sensing location. Each scan took approximately 2 minutes.

In the experiment, 93 fishing bobbers were used as features and were randomly placed in the testing tank as shown by the crosses in Figure 10. The sonar returns from the tank walls were discarded by time gating. The sonar trajectory was set to perform a lawnmower path starting at the lower right corner of the tank and moving towards the left. The estimated result from the DSM algorithm was compared to the true position of the sonar as obtained from position encoders on the robotic positioning system. The entire mission lasted about 1250 time steps. The resulting position estimate errors and the normalized squared state errors for the experiment are shown in Figure 11.

## 7. Conclusion

This paper has presented a new, computationally efficient method for large-scale CML and demonstrated its performance through simulations and experiments. The single-pass and multi-pass DSM algorithms yield performance that is comparable to full covariance stochastic mapping, while maintaining constant computational requirements. Further work is necessary to explore the limits of the approximations employed by the cross-map relocation and cross-map updating submap transition strategies. For example, the normalized squared errors of multi-pass DSM are too large when a repetitive survey path is followed (Figure 8), but are quite good when an alternating survey path is followed (Figure 9). The results are encouraging, however, because they demonstrate successful stochastic mapping on a scale an order of magnitude larger than any results previously published.

Work in progress is investigating alternative submap transition strategies, for example using covariance intersection [7]. Provably consistent error bounds can be achieved at the expense of a linear-time algorithm that maintains current vehicle-to-feature cross-correlation terms for all inactive submaps. Our current and future research aims to achieve a provably consistent, constant-time algorithm that can achieve spatial and temporal convergence, without an undue increase in data association complexity.

## Acknowledgments

This research has been funded in part by the NSF through grant BES-9733040, the MIT Sea Grant College Program under grant NA86RG0074 (project RCM-3), the Naval Undersea Warfare Center under contract N66604-99-M-7235, the Norwegian Research Council through grant 109338/410, and the Henry L.

and Grace Doherty Assistant Professorship in Ocean Utilization. The authors wish to thank Robert Carpenter, Simon Julier, Jeff Uhlmann, Rick Rikoski, and Sung Joon Kim for helpful discussions and comments.

## References

- [1] R. A. Brooks. Aspects of mobile robot visual map making. In *Second Int. Symp. Robotics Research*, Tokyo, Japan, 1984. MIT Press.
- [2] R. Chatila and J.P. Laumond. Position referencing and consistent world modeling for mobile robots. In *IEEE International Conference on Robotics and Automation*. IEEE, 1985.
- [3] M. W. M. G. Dissanayake, P. Newman, H. F. Durrant-Whyte, S. Clark, and M. Csorba. A solution to the simultaneous localization and map building (SLAM) problem. In *Sixth International Symposium on Experimental Robotics*, March 1999.
- [4] R. Smith, M. Self, and P. Cheeseman. A stochastic map for uncertain spatial relationships. In *4th International Symposium on Robotics Research*. MIT Press, 1987.
- [5] P. Moutarlier and R. Chatila. Stochastic multisensory data fusion for mobile robot location and environment modeling. In *5th Int. Symposium on Robotics Research*, Tokyo, 1989.
- [6] J. J. Leonard and H. F. Durrant-Whyte. Simultaneous map building and localization for an autonomous mobile robot. In *Proc. IEEE Int. Workshop on Intelligent Robots and Systems*, pages 1442–1447, Osaka, Japan, 1991.
- [7] J. K. Uhlmann, S. J. Julier and M. Csorba. Nondivergent Simultaneous Map Building and Localisation using Covariance Intersection. *Navigation and Control Technologies for Unmanned Systems II*, 1997.
- [8] J. A. Castellanos, J. D. Tards, and G. Schmidt. Building a global map of the environment of a mobile robot: The importance of correlations. In *Proc. IEEE Int. Conf. Robotics and Automation*, pages 1053–1059, 1997.
- [9] R. N. Carpenter. Concurrent mapping and localization using forward look sonar. In *IEEE AUV*, Cambridge, MA, August 1998.
- [10] H. J. S. Feder, C. M. Smith, and J. J. Leonard. Incorporating environmental measurements in navigation. In *IEEE AUV*, Cambridge, MA, August 1998.
- [11] H. J. S. Feder, J. J. Leonard, and C. M. Smith. Adaptive mobile robot navigation and mapping. *Int. J. Robotics Research*, 18(7):650–668, July 1999.
- [12] J. J. Leonard and H. J. S. Feder. Decoupled stochastic mapping. Marine Robotics Laboratory Technical Report 99-1, Massachusetts Institute of Technology, 1999.
- [13] Y. Bar-Shalom and X. R. Li. *Estimation and Tracking: Principles, Techniques, and Software*. Artech House, 1993.

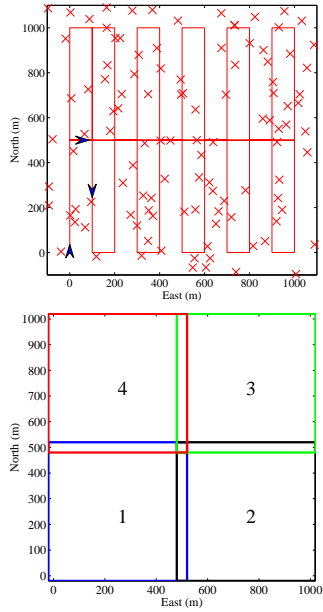


Figure 4: *Top*: the desired survey path of the vehicle and the location of the 110 randomly distributed point features (crosses). The vehicle starts at (0,0) meters and follows the path of the arrows. *Bottom*: the submap partition of the survey area as generated by the two DSM algorithms.

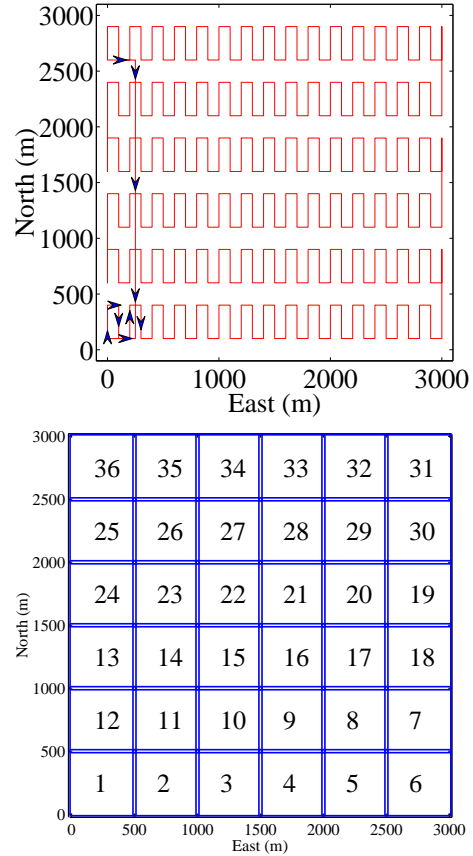


Figure 6: *Top*: The desired survey path of the vehicle in the 3 km by 3 km survey area with 1200 features. *Middle*: The partition of the survey area into 36 submaps. *Bottom*: The true feature positions (marked by 'x') and the estimated feature positions (marked by '+') and  $3\sigma$  error ellipses for the long duration multi-pass DSM run.

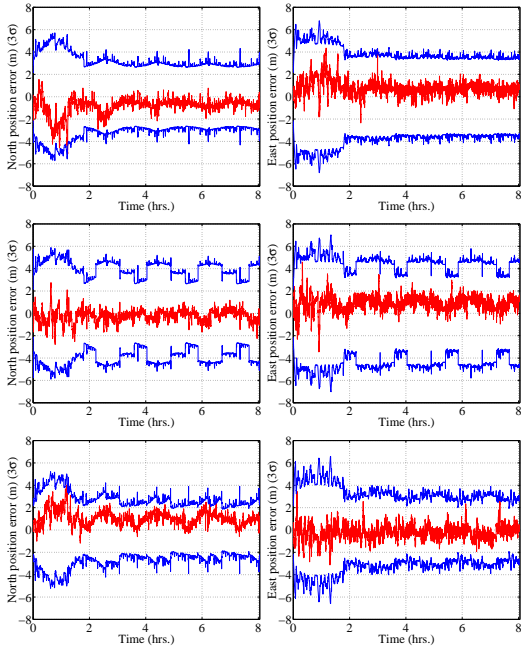


Figure 5: Errors and  $3\sigma$  bounds produced by full covariance ASM(top), single-pass DSM (middle), and multi-pass DSM (bottom) surveys of the region shown in Figure 4

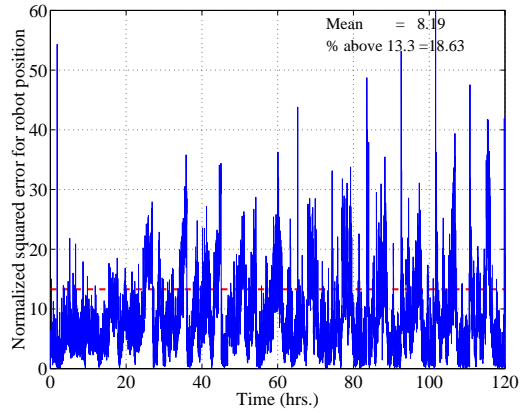
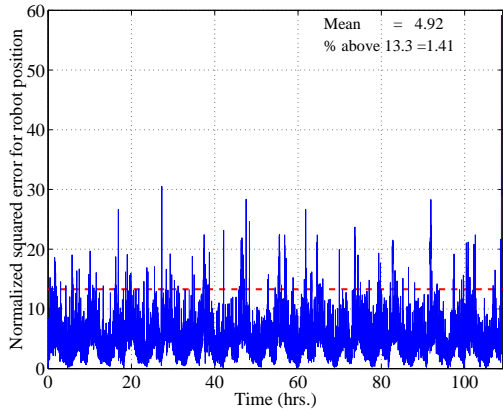
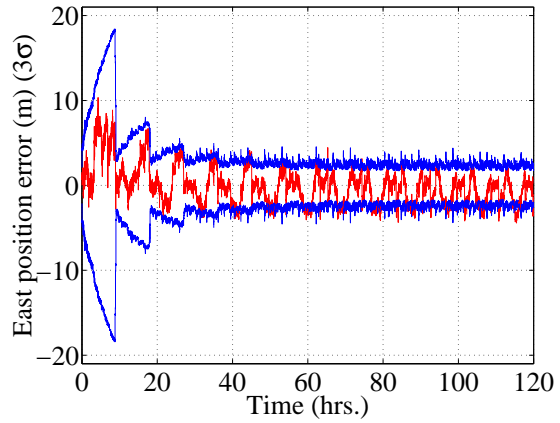
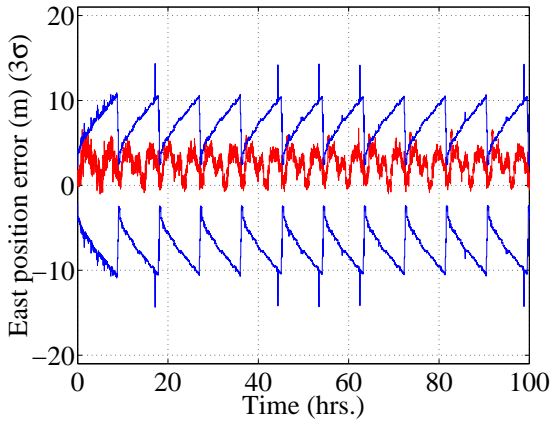
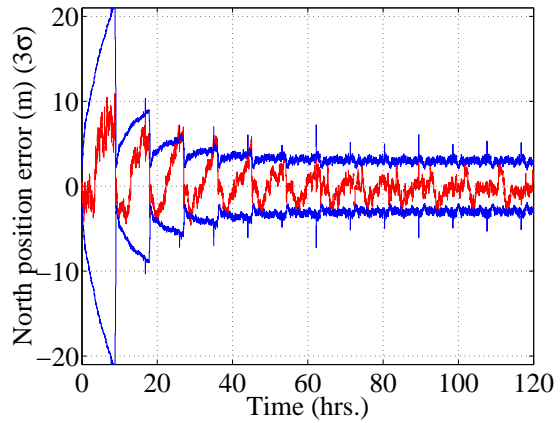
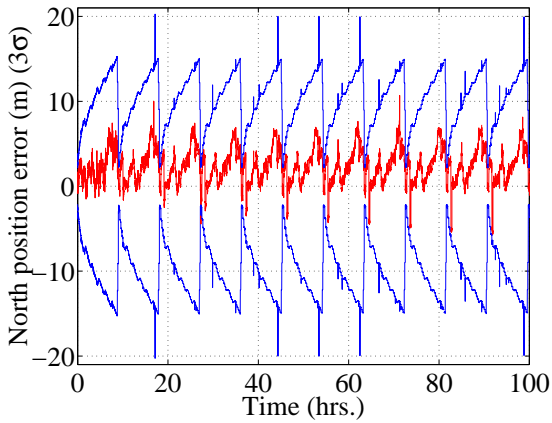


Figure 7: Position errors,  $3\sigma$  bounds (top and middle), and normalized mean squared error (bottom) for a 36 submap single-pass DSM survey of the area given in Figure 6. The horizontal dashed line drawn at the value 13.3 in the bottom plot indicates the 99% error level [13].

Figure 8: Position errors,  $3\sigma$  bounds (top and middle), and normalized mean squared error (bottom) for a 36 submap multi-pass DSM survey of the area given in Figure 6. The horizontal dashed line drawn at the value 13.3 in the bottom plot indicates the 99% error level [13].

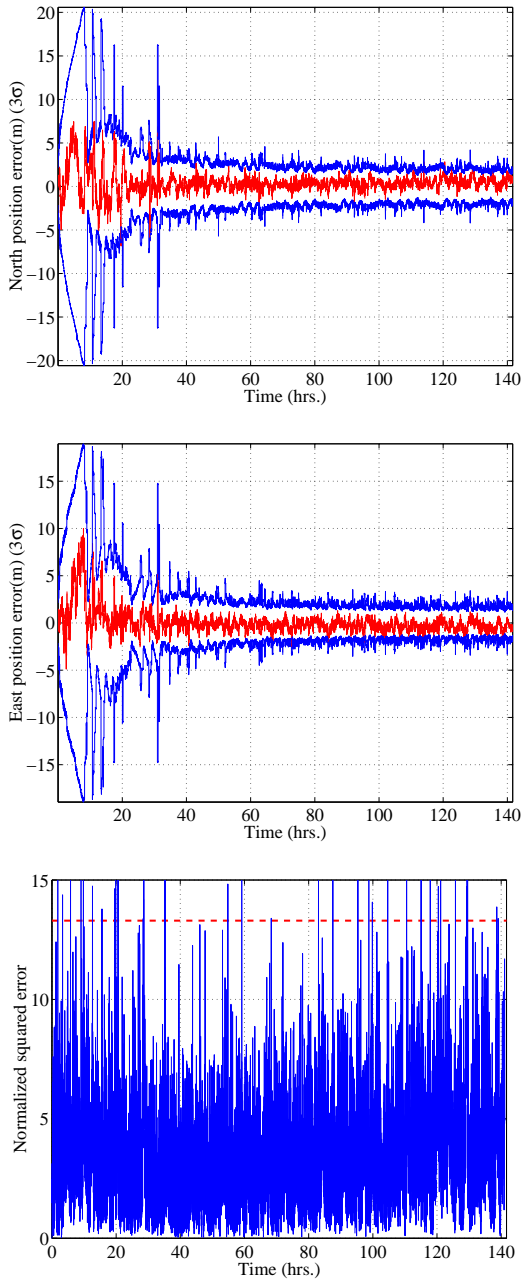


Figure 9: Position errors,  $3\sigma$  bounds (top and middle), and normalized mean squared error (bottom) for a 36 submap multi-pass DSM survey of an environment with 1200 features with the same conditions as in Figure 8, except using an alternating survey strategy that rotates the path given in Figure 6 by 90 degrees after each complete circuit of the environment. The first two cycles through the environment result in the following submap transition sequence: 1, 2, 3, ..., 36, 25, 24, 13, 12, 1, 12, 13, 24, 25, 36, 35, 26, 23, 15, 11, 2, 3, 10, 15, 22, 27, 34, 33, 32, 29, 20, 17, 8, 5, 6, 7, 18, 19, 30, 31. By varying the submap transition sequence in this manner, improved normalized squared errors are obtained.

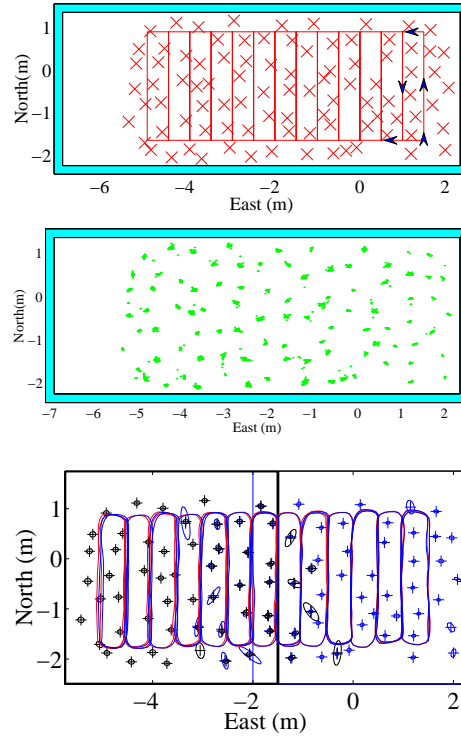


Figure 10: *Top*: Desired path and the location of 93 features for the experiment. *Middle*: All sonar returns processed during the experiment, referenced to the true sensor location. (Returns originating from the tank walls were discarded.) *Bottom*: Actual path of the sensor and estimated feature locations with  $3\sigma$  error ellipses.

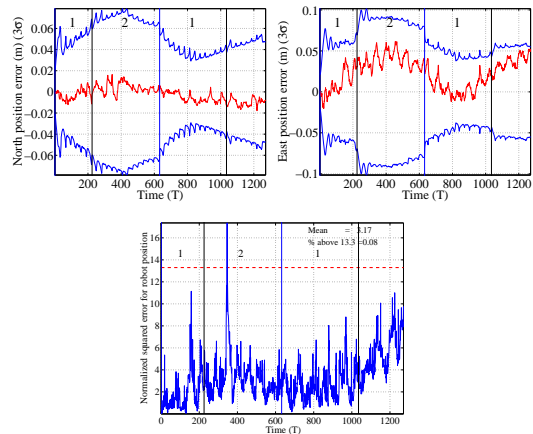


Figure 11: Position errors,  $3\sigma$  bounds (top) and normalized mean squared error (bottom) for the robot position for multi-pass DSM experiment in the testing tank.